Available online at www.sciencedirect.com
ScienceDirect
Trans. Nonferrous Met. Soc. China 29(2019) 1285−1293
Transactions of Nonferrous Metals Society of China
www.tnmsc.cn

Early warning of rock mass instability based on multi-field coupling analysis and microseismic monitoring

Zhou-quan LUO[1], Wei WANG[1], Ya-guang QIN[1], Jun XIANG[2]

1. School of Resources and Safety Engineering, Central South University, Changsha 410083, China;
2. Fankou Lead−Zinc Mine, Shaoguan 512325, China

Received 23 April 2018; accepted 17 April 2019

Abstract: In order to overcome the limitation that rock mass instability warnings are caused by a lack of deep consideration of the inherent mechanism of disaster formation, early warning signs of rock mass instability were detected and multi-field coupling was analyzed. A multi-field coupling model of a damaged rock mass was established. The relationship between microseismic activity parameters and rock mass stability was analyzed, and a multi-parameter early warning index system was established and its solution program was compiled. Based on the D−S data fusion theory, an early warning model of rock mass instability combining multi-field coupling analysis and microseismic monitoring was constructed. Taking an underground mine stope as an object, the multi-field coupling model and its solution program were used to analyze mining response characteristics. The seismic field data were used to verify the accuracy of the multi-field coupling analysis. The early warning model was used to predict the instability of stope rock mass, and the early warning result is consistent with a real-world scenario.

Key words: rock mass instability; microseismic characteristic parameters; D−S evidence fusion; multi-parameter early warning; damage distribution

1 Introduction

Risk factors are associated with underground rock engineering as resource exploitation depths increase. These factors include the probability of roof collapse, water bursts, and rock bursts, all of which pose a significant threat to underground production operations. Rock disasters in underground mines are mostly induced by mining activities, and occur in geological environments that are composed of stress field, seepage field, temperature field, and so on. In addition, rock disasters show complex nonlinear deformation and failure characteristics. From the analysis of the mechanism of disaster inoculation and evolution, rock disasters are developed from mesoscale (small-scale) damage to macroscopic (large-scale) deformation and failure. The occurrence of rock disasters is often accompanied by certain precursory characteristics [1], and it is very important to accurately grasp the law of precursory characteristics in order to obtain reliable early warning indicators, which aid in the control of rock mass disasters.

When rock failure occurs (usually in the form of rock burst, sheet support, roof collapse, etc), it will release energy in the form of elastic waves. Microseismic monitoring technology is the identification and analysis technology of rock mass stability by releasing and analyzing elastic waves released from rock failure. Microseismic monitoring technology is real-time, full range, and has a wide range within the microseismic monitoring technique for the precise positioning of rock failure events. By examining seismic characteristic parameters and analyzing the variation of activity during a rock failure process, we can provide effective support that provides early warning indications that can be used to prevent mass disasters from occurring. Based on microseismic monitoring technology many researches on the monitoring and early warning of rock mass instability have been conducted by scholars at home and abroad.

By analyzing the characteristics of an explosion that occurred before and after a microseismic signal of hard mine rock was detected, LI [2] found that microseismic characteristic parameters accumulated for a period of

Foundation item: Project (2017yfc0602901) supported by the National Key R&D Program of China during the Thirteenth Five-Year Plan Period; Project (2017zzts204) supported by the Fundamental Research Funds for the Central Universities of Central South University, China
Corresponding author: Ya-guang QIN; Tel: +86-15574830243; E-mail: csuqyg@163.com
DOI: 10.1016/S1003-6326(19)65035-1

time before the rock burst occurred, and decreased rapidly before the rock burst approached. Thus, the relation between the variation of action parameters and the instability of rock mass was revealed. By using a tomography method, LURKA [3] evaluated the hidden danger area of the working face of a coal mine, and found that the velocity of the first microseismic break is proportional to the microseismic risk in the monitoring area. By means of microseismic monitoring, SHEN et al [4] obtained the precursor variation rule of displacement and stress in a mine stope roof crossing, and provided a way to predict roof crossing. According to the theory of rock failure and seismology, TANG [5] studied a time series of microseismic activity parameters and the precursory features of a rock burst. LU et al [6] revealed the mathematical relationship between the quantitative characteristics of microseismic parameters and the dynamic failure of rock through experiments, and obtained prediction information of the destruction of rock mass. YU et al [7] combined the distribution characteristics of a microseismic and background stress field and analyzed the accumulation and migration process of stress in a mining rock mass. This analysis was based on a high-performance large-scale scientific computing platform, and a new method was established for obtaining early warning indications of rock mass instability.

At present, early warning indications of rock mass disasters based on microseismic monitoring mainly rely on microseismic parameters. We can explore and establish the relationship between microseismic characteristic parameters and the precursory rule of a rock disaster. In essence, the intrinsic reason why rock disasters occur is the multi-field coupling effect of stress, seepage, and damage, and microseismic monitoring is more external performance. Thus, early warning indications based on microseismic monitoring lack a comprehensive consideration of the inherent mechanism of rock mass disasters. Based on the multi-field coupling simulation analysis, in this study, we conducted research on space-time monitoring and determined early warning indications of rock mass disasters based on microseismic monitoring and multi-field coupling analysis.

2 Multi-field coupling model of rock mass

In order to simplify the expression of the formula, this study adopts the abstract notation of a tensor. The definitions of the rock stress tensor $\boldsymbol{\sigma}$ sigma and strain tensor $\boldsymbol{\varepsilon}$, based on the assumptions of small deformation, equilibrium equations, and geometric equations of rock mass are as follows:

$$\begin{cases} \nabla \cdot \boldsymbol{\sigma} + \boldsymbol{F} = 0 \\ \boldsymbol{\varepsilon} = (\nabla \boldsymbol{u} + \boldsymbol{u}\nabla)/2 \end{cases} \tag{1}$$

where ∇ is the Laplace operator, $\boldsymbol{F}$ is the volume force tensor, and $\boldsymbol{u}$ is the displacement tensor.

It is generally believed that the internal seepage of a rock mass is incompressible and obeys Darcy's law:

$$\begin{cases} \nabla \cdot \boldsymbol{v} = Q_{\mathrm{m}} \\ \boldsymbol{v} = -\dfrac{(\nabla p + \rho g h)}{\mu}\boldsymbol{K} \end{cases} \tag{2}$$

where $\boldsymbol{v}$ is seepage speed vector, Q_{m} is the source item, p is seepage pressure, μ is the dynamic viscosity coefficient of the fluid, ρ is the fluid density, g is gravitational acceleration, h is the velocity head, and $\boldsymbol{K}$ is the permeability tensor.

The conventional multi-field coupling method is mainly based on the Biot consolidation equation [8]; that is, the coupling of stress and seepage through effective stress principle and volume strain source term:

$$\begin{cases} \boldsymbol{\sigma}' = \boldsymbol{C} : \varepsilon - \alpha p \\ Q_{\mathrm{m}} = -\dfrac{\partial \varepsilon_{\mathrm{v}}}{\partial t} \end{cases} \tag{3}$$

where $\boldsymbol{\sigma}'$ is the effective stress tensor, $\boldsymbol{C}$ is the elastic stiffness tensor of the rock mass, α is the effective stress coefficient of Biot, and ε_{v} is the volumetric strain of rock mass.

From the angle of conservation and the transformation of energy [9], the damage variable, D, is defined as follows:

$$D = \frac{U_{\mathrm{d}}}{U} = \frac{U_{\mathrm{d}}}{U_{\mathrm{d}} + U_{\mathrm{e}}} \tag{4}$$

where U_{d} and U_{e} are the dissipative energy and releasable elastic strain energy during the deformation and failure process of the rock mass, respectively.

Introducing the damage variable, D, in Formula (3), the multi-field coupling model considering damage is obtained as follows:

$$\begin{cases} \nabla \cdot \left[\boldsymbol{C}(D) : \left(\dfrac{\nabla \boldsymbol{u} + \boldsymbol{u}\nabla}{2} \right) \right] - \alpha p + \boldsymbol{F} = 0 \\ \nabla \cdot \left[-\dfrac{(\nabla p + \rho g h)}{\mu} \boldsymbol{K}(D) \right] + \dfrac{\partial \varepsilon_{\mathrm{v}}}{\partial t} = 0 \end{cases} \tag{5}$$

In the improved multi-field coupling model, by considering the damage elastic stiffness tensor and permeability tensor, $\boldsymbol{C}(D)$ and $\boldsymbol{K}(D)$, we can express the effect of stress and seepage damage. In addition, αp in the rock constitutive equation expresses the effective stress effect of seepage, and the bulk strain source, $\partial \varepsilon_{\mathrm{v}}/\partial t$, expresses the rock mass effect of deformation on seepage continuity. The coupling action of stress, seepage, and damage is taken into account in the improved model.

The improved multi-field coupling model is constructed by using a set of differential equations that include multiple dependent variables while considering the heterogeneity of rock mass strength parameters and seepage anisotropy. The model is highly nonlinear and the coupling relation is very complex. It is difficult to obtain an analytic solution by means of series variation or integration. Therefore, the improved multi-field coupling model is solved using a numerical method. COMSOL Multiphysics is a finite element numerical analysis software program designed specifically to solve multi-field coupling problems. It also provides powerful programming functions. Based on the COMSOL numerical platform, a program for improving the multi-field coupling model is developed using the Matlab M programming language.

3 Relationship between microseismic parameters and rock stability

Seismology serves as the theoretical basis for the quantitative analysis of microseismic events. According to the analysis of microseismic events, the stability of a rock mass can be evaluated. At present, the main microseismic analysis parameters are the energy index, EI, the Schmidt number, Sc_s, and the apparent volume, V_A. The equations for these parameters are defined as follows [10]:

$$\begin{cases} EI = E/\overline{E}(M) \\ Sc_s = \dfrac{4\mu_1^2 \Delta V \Delta t(\overline{t}) \sum_{t_1}^{t_2} E}{\rho(\overline{X})^2 \left(\sum_{t_1}^{t_2} M_{ij} \right)^2} \\ V_A = \dfrac{M^2}{2\mu_1 E} \end{cases} \tag{6}$$

where $\overline{t}$ is the average time between adjacent micro-earthquakes, μ_1 is the shear stiffness of the rock mass, ρ is the rock mass density, $\overline{X}$ is the average distance between adjacent microearthquakes, M is the seismic moment, E is the microseismic event energy, and $\overline{E}(M)$ is determined by the relation curve of $\lg E$ and $\lg M$ in space area ΔV.

According to the definition of Formula (6), the energy index reflects the ratio of the energy to the average energy of a microseismic event, and an increase in the energy index indicates the storage and the accumulation of energy. The apparent volume reflects the degree of deformation of the rock mass, and the greater the apparent volume is, the greater the deformation of the rock mass is. The Schmidt number is essentially the ratio of the kinematic viscosity to the diffusion rate, and it can reflect the temporal and spatial complexity of the rheology of the rock mass. In general, the variation of microearthquake parameters can be analyzed with the full stress−strain curve of the rock. The initial stage of the strain of the rock is the strain hardening stage, which corresponds to the slow increase in the energy index and the apparent volume of the microearthquake. Before the rock mass reaches its peak strength, the energy index and the apparent volume show a steady growth trend. After the peak strength of the rock mass is reached, the rock bearing capacity decreases because of the deformation and failure of rock mass, the stress inside the rock decreases, and the deformation increases. This reaction is illustrative of strain softening characteristics. Correspondingly, the energy index drops, the apparent volume rises, and the Schmidt number drops faster, indicating that the deformation of the rock mass is more unstable. According to the variation characteristics of microseismic activity parameters, we can judge the stability of rock mass, especially when these parameters change abnormally.

4 Early warning model of rock mass instability

The microseismic monitoring parameters (energy index, Schmidt number, and apparent volume), mining stress index, and damage variable index were selected to establish a multi-parameter early warning index system of rock mass instability.

Based on the D−S evidence theory [11], a model for multi-parameter monitoring and early warning of an unstable rock mass is developed by combining the microseismic monitoring index with the multi-field coupling index. This method is executed as follows:

(1) Determining identification framework

Identify the risk identification framework in the mining area, $\Theta=\{A, B, C\}$, where A indicates that the object area is not dangerous, B indicates that the object area is at medium risk, and C represents a high-risk object region.

(2) Obtaining evidence

Different early-warning indicators are used as evidence to carry out a basic credibility distribution. In this study, A, B, and C risk levels in the identification framework are regarded as fuzzy sets, and the membership functions of A, B, and C are constructed as follows:

$$\mu_A(S) = \begin{cases} 1, \ S < a \\ \dfrac{a+b-2S}{b-a}, \ a \le S < \dfrac{a+b}{2} \\ 0, \ S \ge \dfrac{a+b}{2} \end{cases} \tag{7}$$

$$\mu_B(S)=\begin{cases}0,\ S<a \text{ or } S\ge b\\ \dfrac{2S-2a}{b-a},\ a\le S<\dfrac{a+b}{2}\\ \dfrac{2b-2S}{b-a},\ \dfrac{a+b}{2}\le S<b\end{cases} \tag{8}$$

$$\mu_C(S)=\begin{cases}0,\ S<\dfrac{a+b}{2}\\ \dfrac{2S-a-b}{b-a},\ \dfrac{a+b}{2}\le S<b\\ 1,\ S\ge b\end{cases} \tag{9}$$

where S is the value of early warning indicators, a and b are the critical values chosen by the fuzzy subset of the early warning indicators in the divisions of medium and high risk, respectively. According to the membership function, we can obtain the membership degree of the three risk grades corresponding to A, B, and C, and take the membership degree as the basic reliability of the early warning index.

$$\begin{cases}m_i(A)=\mu_A(S)\\ m_i(B)=\mu_B(S)\\ m_i(C)=\mu_C(S)\end{cases} \tag{10}$$

Using the calculation of the membership function of the evidence body, the results of the basic credibility of the risk grade for the object area are shown in Table 1.

Table 1 Basic credibility assignment of risk grade for object area

Energy index	Apparent volume	Schmidt number	Mining stress	Damage variable
$m_1(A)$	$m_2(A)$	$m_3(A)$	$m_4(A)$	$m_5(A)$
$m_1(B)$	$m_2(B)$	$m_3(B)$	$m_4(B)$	$m_5(B)$
$m_1(C)$	$m_2(C)$	$m_3(C)$	$m_4(C)$	$m_5(C)$

(3) D−S evidence fusion

The process of applying the D−S theory for the fusion of evidence is described as follows [12]: for evidences E_1 and E_2 under identification framework Θ, their basic reliability distribution functions are m_1 and m_2, and the focal elements are A_i and A_j, respectively. The calculation of the similarity coefficient between evidences A and B is described as follows:

$$d_{12}=\frac{\sum\limits_{A_i\cap B_j=A_A\ne\Phi} m_1(A_i)m_2(B_j)}{\sqrt{(\sum m_1^2(A_i))(\sum m_2^2(B_j))}} \tag{11}$$

d_{12} is used to describe the similarity between E_1 and E_2, and the value range of d_{12} is [0,1]. The greater the d_{12} value is, the better the certainty is.

For the amount of evidence collected, n, Formula (11) can calculate the similarity between E_1 and E_2, which can be represented as the following similar matrix:

$$\boldsymbol{S}=\begin{bmatrix}1 & d_{12} & \cdots & d_{1n}\\ d_{21} & 1 & \cdots & d_{2n}\\ \vdots & \vdots & \vdots & \vdots\\ d_{n1} & d_{n2} & \cdots & 1\end{bmatrix} \tag{12}$$

Adding each line of the similar matrix, we can obtain the support of each evidence to E_i:

$$Sup(m_i)=\sum_{j=1}^{n} d_{ij}\quad (i, j=1,2,\cdots,n) \tag{13}$$

To normalize the support of the evidence, the credibility of the evidence can be obtained.

$$Crd(m_i)=\frac{Sup(m_i)}{\sum\limits_{i=1}^{n} Sup(m_i)}\qquad (i, j=1,2,\cdots n) \tag{14}$$

The sum of each trustworthiness is 1, which is used as the weight of the evidence, E_i. The weighted average reliability value of the identification frame index can be calculated by the basic credibility of the evidence and the corresponding weight.

$$m(A)=\sum_{i=1}^{h} m_i(A)Crd(S_i) \tag{15}$$

(4) Early warning analysis

After using the D−S theory to obtain the credibility of the early warning indicators, the results are judged by the specified decision rules. In this study, a decision method based on a probability assignment is used to judge the risk grade of the object region.

$$\begin{cases}m(A_1)=\max\left(m(A_i), A_i\subset\Theta\right)\\ m(A_2)=\max\left(m(A_i), A_i\subset\Theta \text{ and } A_i\ne A_1\right)\end{cases} \tag{16}$$

Set the thresholds ε_1 and ε_2, if they meet the conditions:

$$\begin{cases}\varepsilon_1<m(A_1)-m(A_2)\\ m(\Theta)<\varepsilon_2\\ m(\Theta)<m(A_1)\end{cases} \tag{17}$$

A_1 is the result of the risk grade.

5 Engineering application

5.1 Engineering situation

An underground mining area is located between −400 m level and −360 m level sections. The stope ore reserves are approximately 22200 t, the lower ore average angle is 55°, and the ore grade (Pb + Zn) is 14%. The regional strata is D3ta, and the main lithology is deep gray, thick-bedded limestone. A total of six blasting schemes are planned for the stope. The mining method is the column back lateral caving method without a bottom hole, which is composed of the upper hole down a drilling formation, the stope is composed of hollow holes as the initial compensation space, which is formed layer by layer by a ring groove blasting area, and the remaining ore body is mined by lateral cave blasting. The lower part is a non-pillar mining flat type chamber. The ore is transported by remote LHD, and the mined out area is subsequently backfilled.

5.2 Numerical simulation analysis of mining under multi-field coupling

The multi-field coupled mathematical model and its solution program are used to simulate the mining process, and the response characteristics of rock mass, such as mechanics, seepage, and damage, are analyzed.

(1) Stress distribution characteristics

The stope is perpendicular to the direction of the ore body (north−south strike). The east and west sides of the ore body are the ore rock interfaces, and the two northern and southern ore bodies are adjacent to the ore body to be mined. The mechanical response and failure characteristics of stope will directly affect the stoping of the adjacent stope. Therefore, a typical profile of the maximum and minimum principal stress in the trend direction is intercepted, and the stress distribution characteristics are analyzed (the tensile stress is positive and the compressive stress is negative).

As shown in Fig. 1, because of the homogeneity of rock mass strength parameters, the stress field distribution obtained by numerical simulation is also heterogeneous. The excavation causes the redistribution of stress around the stope, mainly due to the stress drop and stress concentration caused by unloading in some areas. The stress concentration area is mainly located at the top and bottom of the stope, and the maximum principal stress is 30.2 MPa. The unloading area is mainly located on the stope side, and the maximum principal stress is 5.81 MPa. Owning to unloading and blasting, a certain range of tensile stress is formed and the maximum tensile stress value is 3.03 MPa (Fig. 1), which exceeds the tensile strength (2.35 MPa) of the surrounding rock. This causes a tensile failure to occur.

(2) Seepage distribution characteristics

A typical seepage characteristic profile is extracted from the strike direction, as shown in Fig. 2. In Fig. 2, the arrow represents the direction of fluid flow, and the digital label corresponds to the seepage contour. The redistribution of seepage pressure around a stope is caused by excavation unloading. The water pressure decreases rapidly and tends to be zero close to the goaf. Under the action of water head pressure difference, the flow is obviously flowing toward the goaf, the isoline of seepage pressure bends toward the goaf, and finally presents a distribution similar to the precipitation funnel type.

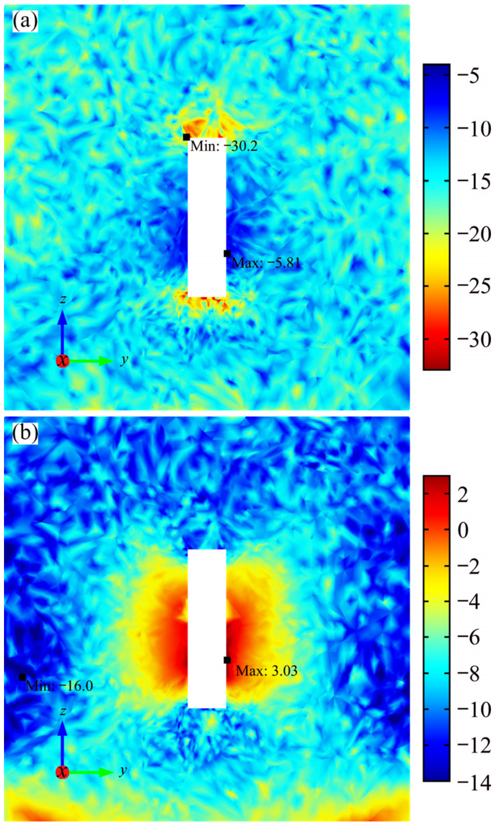

Fig. 1 Distribution characteristics of principal stress (unit: MPa): (a) Maximum principal stress; (b) Minimum principal stress

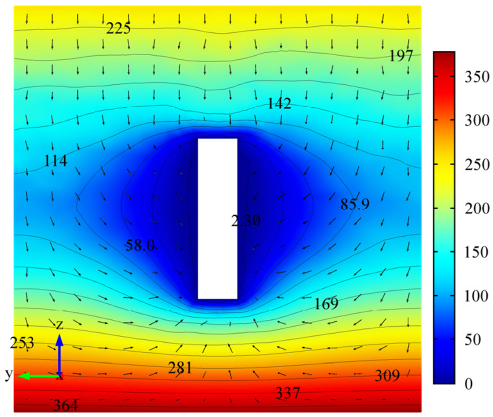

Fig. 2 Seepage pressure distribution and flow path (unit: kPa)

(3) Damage effect analysis

According to the analysis results for stress and seepage, the characteristic points in the direction of mining influence in the strike direction (Fig. 3) are selected, and the changes in their elastic modulus characteristics during excavation are monitored. Deterioration of elastic modulus with damage evolution of monitoring points is shown in Fig. 4, where the deformation strength of the surrounding rock shows a

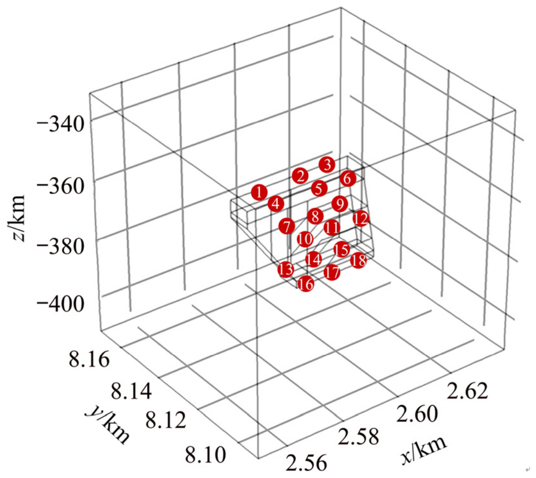

Fig. 3 Three-dimensional display of characteristic monitoring points

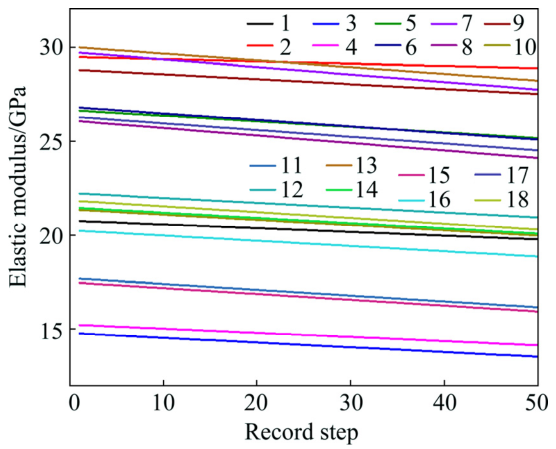

Fig. 4 Deterioration of elastic modulus with damage evolution

downward trend because of the damage caused by excavation. Because of the heterogeneity of the strength parameters, the initial values of the elastic modulus of the monitoring points are different. After excavation, the elastic modulus of the measuring points decreases by 8.7%, with an average decrease of 6.4%. The results of the numerical analysis and field test performed by ZHU et al [13] and JI [14] (excavation area of elastic modulus damage decreasing by an average of 4%−14%) are consistent, which means that the rationality of damage on the strength parameters of rock mass deterioration and damage variable is defined.

5.3 Verification of multi-field coupling simulation results by microseismic monitoring

The damage evolution of a rock mass is an irreversible process of energy dissipation. One part of the input energy of the rock mass is transferred to the elastic strain energy storage of the rock mass; the other part of the input energy dissipates because of the development of internal microcrack rock mass behavior, and spreads out through acoustic emission [15,16]. The multi-field coupling model built in this study is intended to define and consider the impact of damage on rock mass deformation and failure from the perspective of energy. Therefore, in the multi-field coupling analysis, the accumulation of damage corresponds to the occurrence of microseismic events (to a certain extent). Here, the seismic monitoring results are compared with the results obtained by a multi-field coupling simulation. On the one hand, we can use the measured results to further examine multi-field coupling in the model. On the other hand, a multi-field coupling simulation of the stress field, seepage field, or damage response characteristics can be obtained to reveal the precursor law of the disaster. In the multi-field coupling simulation, the damage area of the stope is filtered, and the standard is that the energy dissipated in the damaged area can reach the collection range of the microseismic sensor. As shown in Fig. 5, the distribution of microseismic events in the stope is compared with the damage distribution (microseismic

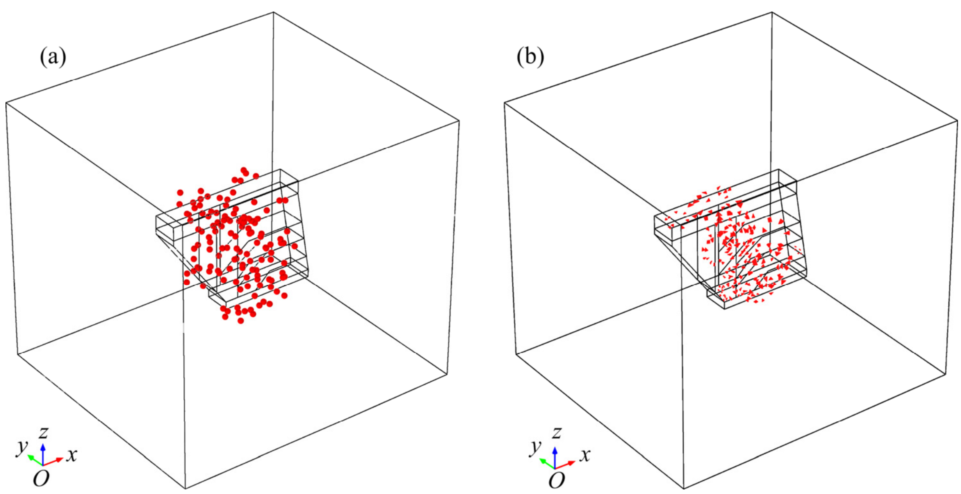

Fig. 5 Comparison of microseismic event distribution (a) and multi-field coupling damage simulation distribution (b)

energy standard) obtained by the multi-field coupling simulation.

As shown in Fig. 5, the distribution of microseismic events is in good agreement with the damage distribution obtained by multi-field coupled simulation, which further verifies the reliability of the multi-field coupling simulation. The multi-field coupling simulation can provide indicators for the mechanism of rock mass disasters, such as mining stress, seepage, and damage response characteristics. Combined with high-precision microseismic monitoring, we can further reveal the precursory rules and characteristics of rock mass instability.

5.4 Early warning application of rock mass instability

The advance warning indices selected in the previous article include the energy index, apparent volume, Schmidt number, mining stress, and the damage variable. According to Table 1, the corresponding basic trustworthiness assignments are $m_1(A, B, C)$, $m_2(A, B, C)$, $m_3(A, B, C)$, $m_4(A, B, C)$, and $m_5(A, B, C)$. The microseismic data from April 8 to April 29, 2017 were selected as the object of study. According to the calculation method of the D−S evidence fusion theory, the variation of the basic credibility of the five early warning bodies of evidence is shown in Fig. 6.

The basic credibility assignment of each index in

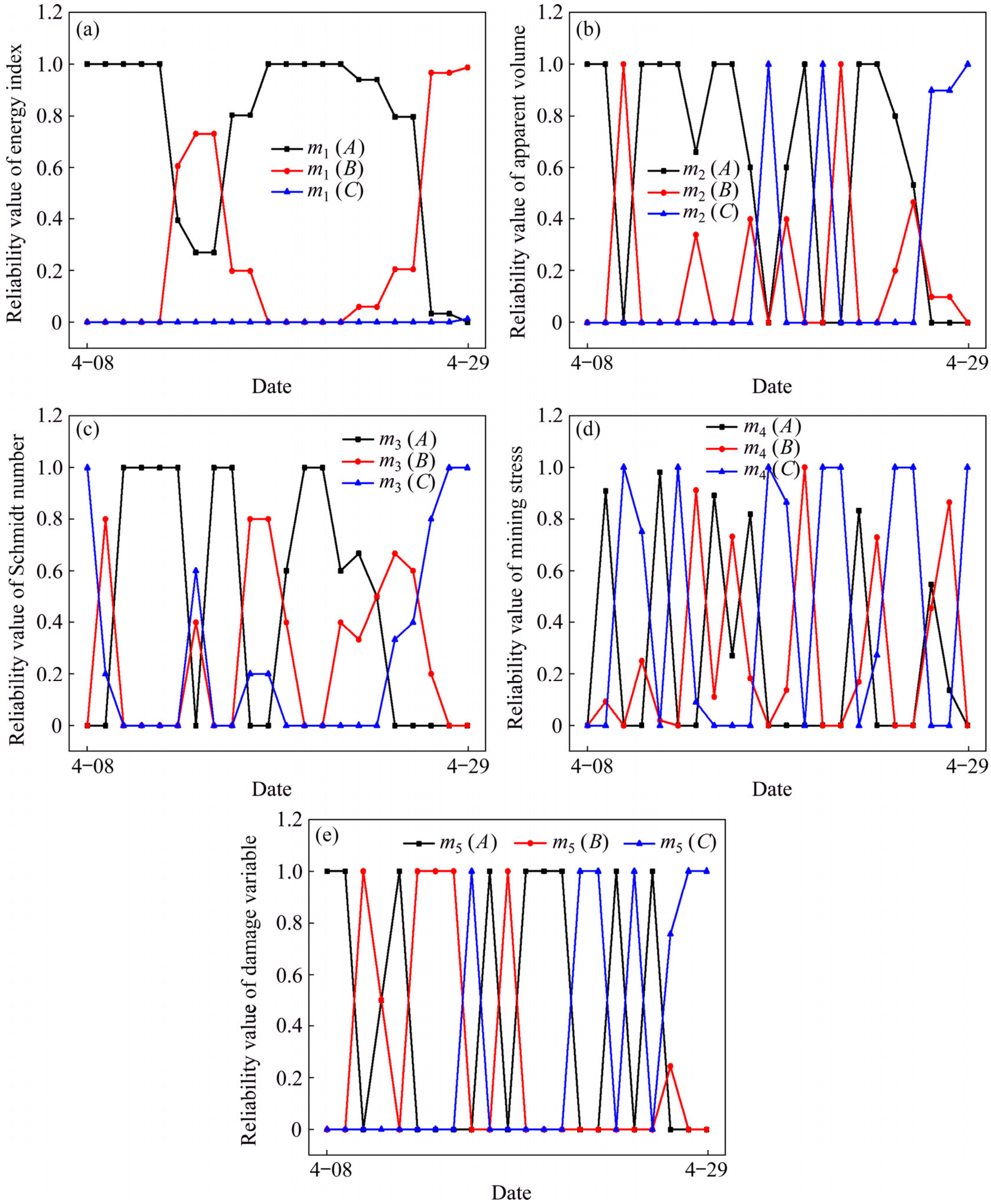

Fig. 6 Temporal variation of basic credibility: (a) Energy index; (b) Apparent volume; (c) Schmidt number; (d) Mining stress; (e) Damage variable

Fig. 6 is weighted together, and a basic probability assignment of evidence fusion is made so as to obtain the early warning results of stope rock mass instability risk, as shown in Fig. 7.

The stope was conducted during the fourth blasting on April 22nd, as shown in Fig. 8. On April 23rd and 24th, the early warning results showed that the rock mass failure probability of the mining area was at medium risk, while on April 25th and 26th, the disaster probability changed to zero risk. On April 27th, the disaster risk increased to a medium risk, and on April 28th and 29th, the disaster risk increased to a high risk level. Based on the early warning results, we can determine that the disaster probability in the adjacent area of the stope was very high after April 27th. The actual situation in the field is as follows: on April 28th, the roof of the roadway in the area fell, there were fresh cracks on the roof of the roadway, and the surrounding workers felt the earthquake. The scene is shown in Fig. 8. Meanwhile, on April 28th, a 0.1 magnitude event was also monitored in the microseismic system. The focal center coordinate is (x: 2606.2 m, y: 8125.6 m, z: −369.5 m), which is located near the caving location. The maximum speed of rock vibration is 7.79 mm/s, which exceeds the threshold of human perception (1 mm/s), and is consistent with the situation observed by field personnel, which detected obvious signs of an earthquake. The field condition and microseismic monitoring indicate that rock mass instability occurs in the stope area, which validates the effectiveness of the early warning model based on multi-field coupling analysis and microseismic monitoring.

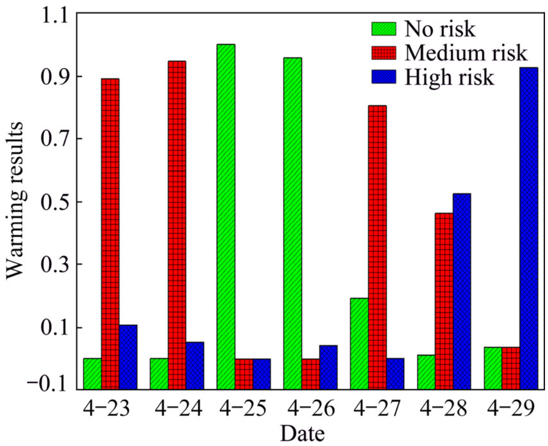

Fig. 7 Early warning results of rock mass instability risk

Fig. 8 Scene photographs of roadway damage in object area: (a) Falling; (b) Roof rupture

6 Conclusions

(1) A multi-field coupling model of damaged rock mass was established and its calculation program was compiled. The mine rock mass characteristics under the multi-field coupling simulation were compared with the microseismic monitoring results, and they were determined to have a good consistency. This verified the validity of the coupling model and showed that the multi-field coupling analysis for rock instability warning is feasible.

(2) Combining a multi-field coupled numerical simulation with high-precision microseismic monitoring, we revealed the mining failure mechanism and precursor rule from a deep level, and established a multi-parameter early warning index system. Based on D−S data fusion theory, an early warning model of rock mass instability was established based on multi-field coupled simulation and microseismic monitoring. The model was used to predict the rock mass instability during the mining process. The early warning result is consistent with the actual situation of the site, which proves the validity of the early warning method.

References

[1] ZHONG D H, WU H, WU B P, ZHANG Y C, YUE P. 3-D fracture network dynamic simulation based on error analysis in rock mass of dam foundation [J]. Journal of Central South University, 2018, 25(4): 919−935.

[2] LI N. Research on mechanisms of key factors and reliability for microseismic source location [D]. Xuzhou: China University of Mining and Technology, 2014. (in Chinese)

[3] LURKA A. Location of high seismic activity zones and seismic hazard assessment in Zabrze Bielszowice coal mine using passive tomography [J]. Journal of China University of Mining and Technology, 2008, 18(2): 177−181.

[4] SHEN B, KING A, GUO H. Displacement, stress and seismicity in roadway roofs during mining-induced failure [J]. International Journal of Rock Mechanics & Mining Sciences, 2008, 45(5): 672−688.

[5] TANG L Z. Study on monitoring and prediction of seismicity and rockburst in a deep mine [D]. Changsha: Central South University, 2008. (in Chinese)

[6] LU C P, DOU L M, WU X R, WANG H M, QIN Y H. Frequency spectrum analysis on microseismic monitoring and signal differentiation of rock material [J]. Chinese Journal of Geotechnical Engineering, 2005, 27(7): 772−775. (in Chinese)

[7] YU Q, TANG C A, LI L C, LI H, CHENG G W. Nucleation process of rockbursts based on microseismic monitoring of deep-buried tunnels for Jinping Ⅱ Hydropower Station [J]. Chinese Journal of Geotechnical Engineering, 2014, 36(12): 2315−2322. (in Chinese)

[8] FERRONATO M, CASTELLETTO N, GAMBOLATI G. A fully coupled 3-D mixed finite element model of Biot consolidation [J]. Journal of Computational Physics, 2010, 229(12): 4813−4830.

[9] LAI Y, LIAO M, KAI H. A constitutive model of frozen saline sandy soil based on energy dissipation theory [J]. International Journal of Plasticity, 2016, 78: 84−113.

[10] ZHAO G Y, MA J, DONG L J, LI X B, CHEN G H, ZHANG C X. Classification of mine blasts and microseismic events using starting-up features in seismograms [J]. Transactions of Nonferrous Metals Society of China, 2015, 25(10): 3410−3420.

[11] FENG R, CHE S, WANG X, YU N. Trust management scheme based on D−S evidence theory for wireless sensor networks [J]. International Journal of Distributed Sensor Networks, 2013, 2013: 1−9.

[12] WU Y, JIAO J, YANG X, XIAO P. Segmentation algorithm for SAR images based on fusion of HMT in the contourlet domain and D−S theory of evidence [J]. Acta Geodaetica et Cartographica Sinica, 2011, 40(2): 148−155.

[13] ZHU Z Q, SHENG Q, ZHANG Y P, LI Y. Research on excavation damage zone of underground powerhouse of Dagangshan hydropower station [J]. Chinese Journal of Rock Mechanics and Engineering, 2013, 32(4): 734−739. (in Chinese)

[14] JI X M. Study on mechanical and hydraulic behavior of tunnel surrounding rock masses in excavation disturbed zone [J]. Chinese Journal of Rock Mechanics and Engineering, 2005, 24(10): 1697−1702. (in Chinese)

[15] DONG L J, LI X B, ZHOU Z L, CHEN G H, MA J. Three-dimensional analytical solution of acoustic emission source location for cuboid monitoring network without pre-measured wave velocity [J]. Transactions of Nonferrous Metals Society of China, 2015, 25(1): 293−302.

[16] HU B, YANG S Q, XU P. A nonlinear rheological damage model of hard rock [J]. Journal of Central South University, 2018, 25(7): 1665–1677.

基于多场耦合分析和微震监测的岩体失稳预警

罗周全[1]，汪 伟[1]，秦亚光[1]，向 军[2]

1. 中南大学 资源与安全工程学院，长沙 410083；

2. 凡口铅锌矿，韶关 512325

摘 要：针对当前岩体失稳预警多从单个角度入手，缺乏对灾害孕育内在机理的深入考虑，开展基于多场耦合分析和微震监测的岩体失稳预警研究。建立考虑损伤的岩体多场耦合模型，并编制相应的解算程序。对微震活动性参数与岩体稳定性之间的关系进行分析，建立多参量预警指标体系。基于 D−S 数据融合理论，构建多场耦合分析和微震监测融合的岩体失稳预警模型。以某地下矿山采场为研究对象，应用多场耦合模型及其解算程序进行采动响应特征分析，运用微震实测数据验证多场耦合分析的正确性。通过构建的预警模型对采场岩体失稳进行预警，预警结果与现场实际情况吻合，验证了预警模型的有效性。

关键词：岩体失稳；微震特征参数；D−S 证据融合；多参量预警；损伤分布

(Edited by Wei-ping CHEN)